Identification of Nanostructural and Specific Absorption Rate (SAR) on $Mn_{0.25}Fe_{2.75}O_4$/Ag Nanoparticle Composites

Identification of Nanostructural and Specific Absorption Rate (SAR) on $Mn_{0.25}Fe_{2.75}O_4$/Ag Nanoparticle Composites

Nadiya Miftachul Chusna[1], Sunaryono[1,2,*], Samsul Hidayat[1], Nurul Hidayat[1], Nandang Mufti[1], Ahmad Taufiq[1,2]

[1]Department of Physics, Faculty of Mathematics and Natural Sciences, Universitas Negeri Malang, Jl. Semarang No. 5, Malang 65145, Indonesia
[2]Research Center of Minerals and Advanced Materials, Faculty of Mathematics and Natural Sciences, Universitas Negeri Malang, Jl. Semarang No. 5 Malang 65145, Indonesia

*Corresponding author: sunaryono.fmipa@um.ac.id

Abstract. $Mn_{0.25}Fe_{2.75}O_4$ nanoparticles have been successfully synthesized using the coprecipitation method. The nanoparticles are the basic components in the fabrication of $Mn_{0.25}Fe_{2.75}O_4$/Ag composites which have been synthesized using the chemical reduction method. To investigate the nanostructure, morphology, functional group, and specific absorption rate (SAR) value of $Mn_{0.25}Fe_{2.75}O_4$ nanoparticles and $Mn_{0.25}Fe_{2.75}O_4$/Ag composites, material has been characterized using XRD, TEM, FTIR, and magneto-thermal instruments respectively. The XRD pattern showed that Mn had been successfully substituted well in the $Mn_{0.25}Fe_{2.75}O_4$ nanoparticles indicated by the shift of diffraction peak towards the smaller angle of 2θ. Through Rietica analysis, the crystal sizes of $Mn_{0.25}Fe_{2.75}O_4$ and Ag nanoparticles were 5.40 nm and 8.05 nm respectively. This result was confirmed well by TEM characteristics which showed that the average size of $Mn_{0.25}Fe_{2.75}O_4$ and Ag particles as much as 5.03 nm and 8.74 nm respectively. The success of Ag nanoparticle in $Mn_{0.25}Fe_{2.75}O_4$/Ag composites was from the distribution of Fe-O and amine functional groups which were the representation of $Mn_{0.25}Fe_{2.75}O_4$ and Ag nanoparticles. Furthermore, Ag nanoparticles were relatively effective in increasing the SAR value of $Mn_{0.25}Fe_{2.75}O_4$/Ag composites of 0.19 W/g (without Ag) into 0.21 W/g (with 0.2 g Ag).

Keywords: Composite, Nanoparticle, $Mn_{0.25}Fe_{2.75}O_4$/Ag, SAR.

1. Introduction

In the 21st century, the research development in the material field becomes an interesting study for many researchers [1]. One of the materials in demand to be studies is a magnetic material. Magnetic material such as magnetite (Fe_3O_4) is multifunctional material which is able to be applied to the industrial, medic, and health fields, among them, are artificial muscles [2], sensor [3], drug production [4], antibacterial [5], antifungal [6], antitoxin [7], hyperthermia therapy [8], and others. In order to be applied to certain types of materials, the magnetic material must be engineered and modified in terms of its size, structure, texture, and material composition so that it has the desired unique properties.

The engineering of Fe_3O_4 nanoparticles has been successfully reported by several researchers regarding its application potential on the biomedical field. Among them, Fe_3O_4 nanoparticles can be increased in temperature until it reaches 47 °C through the influence of AC magnetic field and is predicted to be able to kill cancer cells when the sample is placed in the body area exposed to cancer [8]. Another report also revealed that the specific absorption rate (SAR) of magnetic nanoparticles could reach the numbers of 3,7-325 W/g under the influence of a specific magnetic field on the frequency range of 123-430 kHz which is able to be applied to hyperthermia therapy [9]. Besides, magnetic material engineering by compositing the Fe_3O_4 material with nontoxic materials such as Ag nanoparticles to be applied in the biomedical field also successfully reported by several researchers [10-14]. Fe_3O_4/Ag nanoparticle composites are significant potential to be applied on the biomedical field as an antitoxic material [15], antibacterial [16] and antifungal [17]. However, the research on engineering Fe_3O_4/Ag nanoparticle composites with Mn doping and its potential for medical applications such as hyperthermia therapy is still scarcely conducted. Thus, synthesis of Fe_3O_4/Ag nanoparticle composites with Mn doping is interesting to be conducted. In this research, Mn atom doping in Fe_3O_4 nanoparticles was chosen using a concentration as much as 25% of the sample composition. The doping composition was the optimum saturation magnetization of $Mn_{0.25}Fe_{2.75}O_4$ nanoparticles substituted by Mn atom [18].

The characterization of nanostructure and SAR value of $Mn_{0.25}Fe_{2.75}O_4$/Ag composites was conducted and analyzed more deeply to determine the effectiveness of doping Mn atoms and fillers of Ag nanoparticles in their potential applications for hyperthermia therapy. Through magneto-thermal characterization, the pattern of increasing temperature and SAR values of $Mn_{0.25}Fe_{2.75}O_4$/Ag composites will be further discussed in this report.

2. Methods

2.1. Synthesis of $Mn_{0.25}Fe_{2.75}O_4$/Ag Nanoparticle Composite

The materials used in this research were iron sand taken from Sine beach, Tulungagung, Indonesia. The iron sand was separated using permanent magnet until Fe_3O_4 particle with around 30% of impurity was generated. Fe_3O_4 particles as the separation results were dissolved in hydrochloric acid with a certain composition and stirrer on a magnetic stirrer hotplate at room temperature for 30 minutes. The stirred solution was then filtered using filter paper to obtain a solid black solution. Next, the solution mixed with manganese (II) chloride tetrahydrate and titrated with ammonium hydroxide. The mixing results were deposited and washed using distilled water until $Mn_{0.25}Fe_{2.75}O_4$ nanoparticles were obtained.

The composite process of $Mn_{0.25}Fe_{2.75}O_4$/Ag nanoparticles was initiated with the sonification process of $Mn_{0.25}Fe_{2.75}O_4$ nanoparticles and distilled water for 10 minutes. The solution as the sonification result was then mixed with silver nitrate and stirred using hotplate magnetic stirrer at the temperatures ranged between 343–363 K. Furthermore, $Mn_{0.25}Fe_{2.75}O_4$ nanoparticle composites and silver nitrate were reduced and proceeded with titration of ammonium hydroxide until the pH of the solution reached 11. The process was ended by washing the sample to normal pH and producing $Mn_{0.25}Fe_{2.75}O_4$/Ag nanoparticle composites.

2.2. Characterization of $Mn_{0.25}Fe_{2.75}O_4$/Ag Nanoparticle Composites

The characterization of Ag, Fe_3O_4 and $Mn_{0.25}Fe_{2.75}O_4$ nanoparticle structures were conducted using the XRD Philips X-pert MPD instruments. The data of characterization results were analyzed using Rietica software to determine the crystal size, lattice parameter, and particle size of Ag, Fe_3O_4, $Mn_{0.25}Fe_{2.75}O_4$, and $Mn_{0.25}Fe_{2.75}O_4$/Ag samples. To confirm the sizes of $Mn_{0.25}Fe_{2.75}O_4$/Ag nanoparticle composites, the samples were characterized using Transmission Electron Microscopy (TEM) from JEM1400 JEOL. In addition, samples were also characterized using the Fourier Transform Infra-Red (FTIR) Shimadzu Brand, IRPrestige Type 21. This characterization aimed to reveal the energy absorbed by each functional group of constituent compounds of $Mn_{0.25}Fe_{2.75}O_4$/Ag nanoparticle

composites. Through the absorbed energy content, it could be determined what compounds were contained in the samples.

To obtain the SAR value, $Mn_{0.25}Fe_{2.75}O_4$/Ag, samples were characterized using magneto-thermal instrument. This tool was equipped with electromagnetic which can be controlled frequency so it would generate energy changes received by the sample. The energy absorbed by the sample would change the temperature of the sample until a certain time interval. The pattern of changing the temperature of the sample for this time interval was then obtained to obtain the SAR value of $Mn_{0.25}Fe_{2.75}O_4$/Ag nanoparticle composites. The characteristics of SAR value obtained will give important information from the samples as a potential material for hyperthermia therapy application.

3. Results and Discussion

3.1. X-Ray Diffractions Characterization

Figure 1(a) is the X-ray diffraction pattern of Fe_3O_4 and $Mn_{0.25}Fe_{2.75}O_4$ samples, while Figure 1(b) is the magnification of the highest peak of Fe_3O_4 and $Mn_{0.25}Fe_{2.75}O_4$ phases. All XRD data were analyzed and refined using Rietica software. The refinement results showed that the crystal lattice parameter for Fe_3O_4 and $Mn_{0.25}Fe_{2.75}O_4$ nanoparticles were 8.36 Å and 8.40 Å respectively. The lattice parameter of $Mn_{0.25}Fe_{2.75}O_4$ nanoparticles tended to be bigger than Fe_3O_4 nanoparticles. This is caused by Mn^{2+} cation has a bigger diameter which was ~0.89 Å than Fe^{2+} cation which was ~0.77 Å and Fe^{3+} cation which was ~0.64 Å [19], accordingly the crystal lattice parameter of Fe_3O_4 nanoparticles with doping Mn would be greater than without doping Mn. This result corresponded to the research conducted by several previous researchers who reported that the lattice parameters of Fe_3O_4 nanoparticles experienced an increase when Mn doping was performed [19–22].

Furthermore, the increase in lattice parameter of Fe_3O_4 nanoparticles doped with Mn affected the shift of peaks in the X-ray diffraction pattern towards the smaller 2-theta angle as shown in Figure 1(b). This shift indicates that the lattice parameters of $Mn_{0.25}Fe_{2.75}O_4$ nanoparticles are larger than Fe_3O_4 nanoparticles. This result is in accordance with the Bragg Law equation which says that the lattice parameters of the particle crystal structure are inversely proportional to the change in 2-theta angle [23]. Besides, shifts in the diffraction peaks of $Mn_{0.25}Fe_{2.75}O_4$ nanoparticles towards the smaller 2-theta angle showed that Mn^{2+} cation effectively substituted Fe^{3+} cation position in the Mn doping process to synthesize $Mn_{0.25}Fe_{2.75}O_4$ nanoparticles.

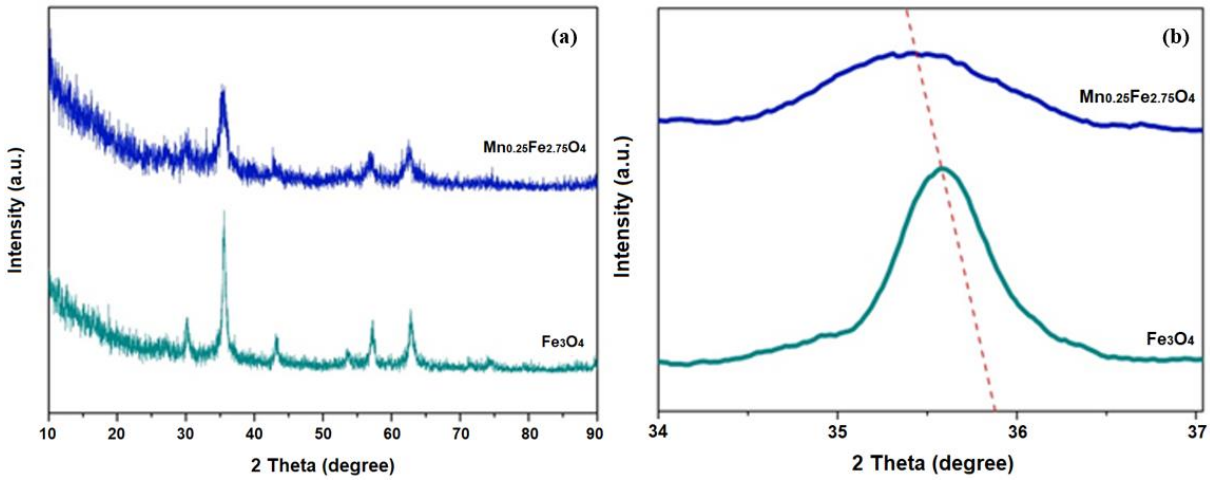

Figure 1. The X-ray diffraction pattern of (a) Fe_3O_4 and $Mn_{0.25}Fe_{2.75}O_4$ samples, and (b) magnification on the highest peak of Fe_3O_4 and $Mn_{0.25}Fe_{2.75}O_4$ phases

The characterization of crystal nanostructure was also performed to Ag, $Mn_{0.25}Fe_{2.75}O_4$, and $Mn_{0.25}Fe_{2.75}O_4$/Ag particles as shown in Figure 2. In Figure 2, the entire diffraction peak $Mn_{0.25}Fe_{2.75}O_4$/Ag (Figure 2 above) is a representation of the combination of Ag nanoparticle diffraction peaks (Figure 2 below) and diffraction peaks of $Mn_{0.25}Fe_{2.75}O_4$/Ag nanoparticles (Figure 2 middle part). This indicated that $Mn_{0.25}Fe_{2.75}O_4$ nanoparticle composites and Ag nanoparticle composites could be produced well. This result is also in accordance with previously published reports [24] - [26]. Through refinement using Rietica software, the results of XRD data analysis on $Mn_{0.25}Fe_{2.75}O_4$/Ag composites generated the average crystal size for $Mn_{0.25}Fe_{2.75}O_4$ and Ag phases were 5.40 nm and 8.05 nm respectively.

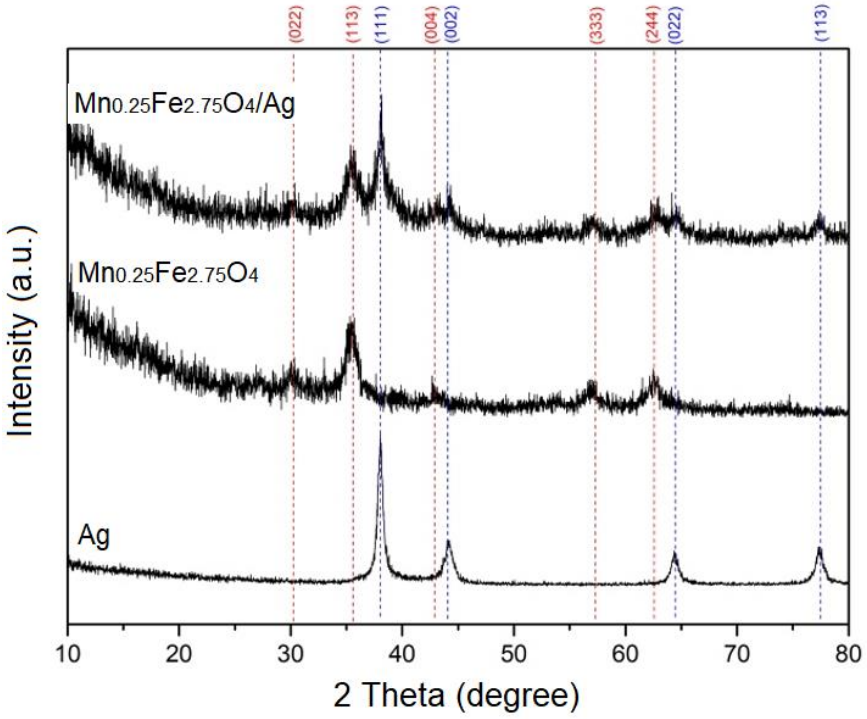

Figure 2. The XRD pattern of Ag, $Mn_{0.25}Fe_{2.75}O_4$, and $Mn_{0.25}Fe_{2.75}O_4$/Ag nanoparticles.

3.2. FTIR Characterization

The FTIR characterization profile for $Mn_{0.25}Fe_{2.75}O_4$ and $Mn_{0.25}Fe_{2.75}O_4$/Ag nanoparticles is shown in Figure 3. From the vibration pattern for the low wavelength, the energy absorption of the two samples occurs in the wavenumbers ranged between 417-585 cm^{-1}. The range of wavelengths is characteristic of the functional group of Fe-O bound [27]. Meanwhile, specifically vibration at the wavenumber of 522 cm^{-1} showed Fe-O vibration which occupied tetrahedral part [28], where most likely Mn^{2+} cation replaced the composition of Fe^{2+} cation [20]. The vibration due to Fe-O also occurred at the wavenumber of 631 cm^{-1} [29,30], and 1356 cm^{-1} [29].

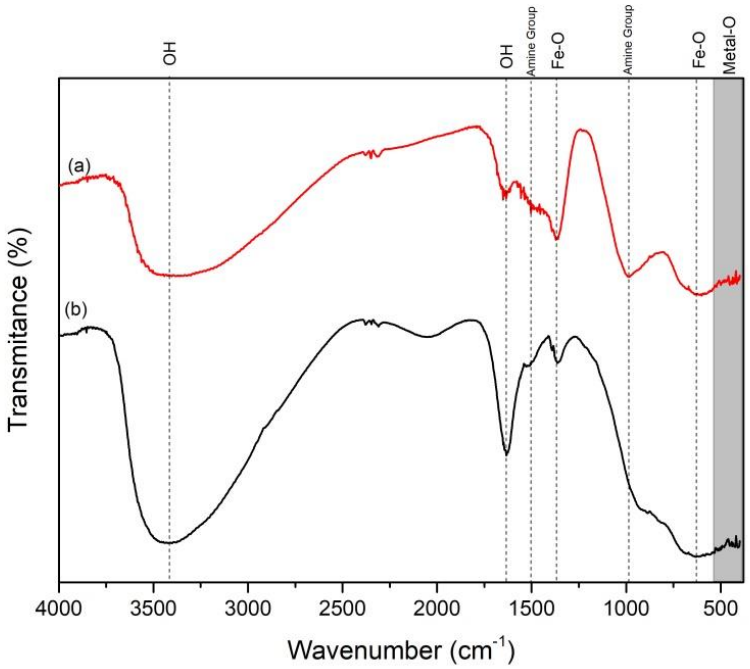

Figure 3. FTIR characterization of sample (a) $Mn_{0.25}Fe_{2.75}O_4$ and (b) $Mn_{0.25}Fe_{2.75}O_4$/Ag

The energy absorption of both samples also occurred at the wavenumbers of 1631 cm^{-1} and 3455 cm^{-1} [28], [31], where the wavenumber corresponds to the O-H bond function group. This shows that both samples are still indicated to contain water. Besides, energy absorption for $Mn_{0.25}Fe_{2.75}O_4$/Ag nanoparticles was clearly seen at the wavenumbers of 992 and 1516 cm^{-1} as shown in Figure 3(b). This energy uptake signifies the amine group caused by a reduction agent in the synthesis process of Ag, ammonium hydroxide solution. Thus, all energy uptake shown in Figure 3 is well identified and in accordance with the functional group bonds of each sample constituent bond.

3.3. TEM Characterization

TEM characterization on $Mn_{0.25}Fe_{2.75}O_4$/Ag composites with 20 nm scale bar were presented in Figure 4(a). Also, the distribution of $Mn_{0.25}Fe_{2.75}O_4$ and Ag material articles sizes respectively are presented in Figures 4 (b) and 4 (c). In Figure 4 (a) it appears that Ag nanoparticles (with yellow marks) appeared to be darker than $Mn_{0.25}Fe_{2.75}O_4$ nanoparticles. Ag nanoparticles were evenly distributed and composited in $Mn_{0.25}Fe_{2.75}O_4$ nanoparticles. The condition and shape of Ag nanoparticles in magnetic nanoparticle composites is in line with the research that has been done by Venkateswarlu *et al.* [31].

Based on the data analysis of $Mn_{0.25}Fe_{2.75}O_4$/Ag composite morphology, it was obtained the mean size of $Mn_{0.25}Fe_{2.75}O_4$ and Ag material particles as much as 5.03 nm and Ag 8.74 nm respectively as shown in the histogram of $Mn_{0.25}Fe_{2.75}O_4$ nanoparticle size distribution (Figure 4(b)) and Ag (Figure 4(c)). This result corresponds to the results of characterization using XRD as discussed earlier, namely the average crystal size for $Mn_{0.25}Fe_{2.75}O_4$ and Ag phases as much as 5.40 nm and 8.05 nm respectively. Thus, the Ag nanoparticle filler distribution is in the matrix of $Mn_{0.25}Fe_{2.75}O_4$ nanoparticles. It can be concluded that it is spread well as evidenced by the morphological results of $Mn_{0.25}Fe_{2.75}O_4$/Ag composites and accuracy of filler size and its matrix from the XRD and TEM data analysis.

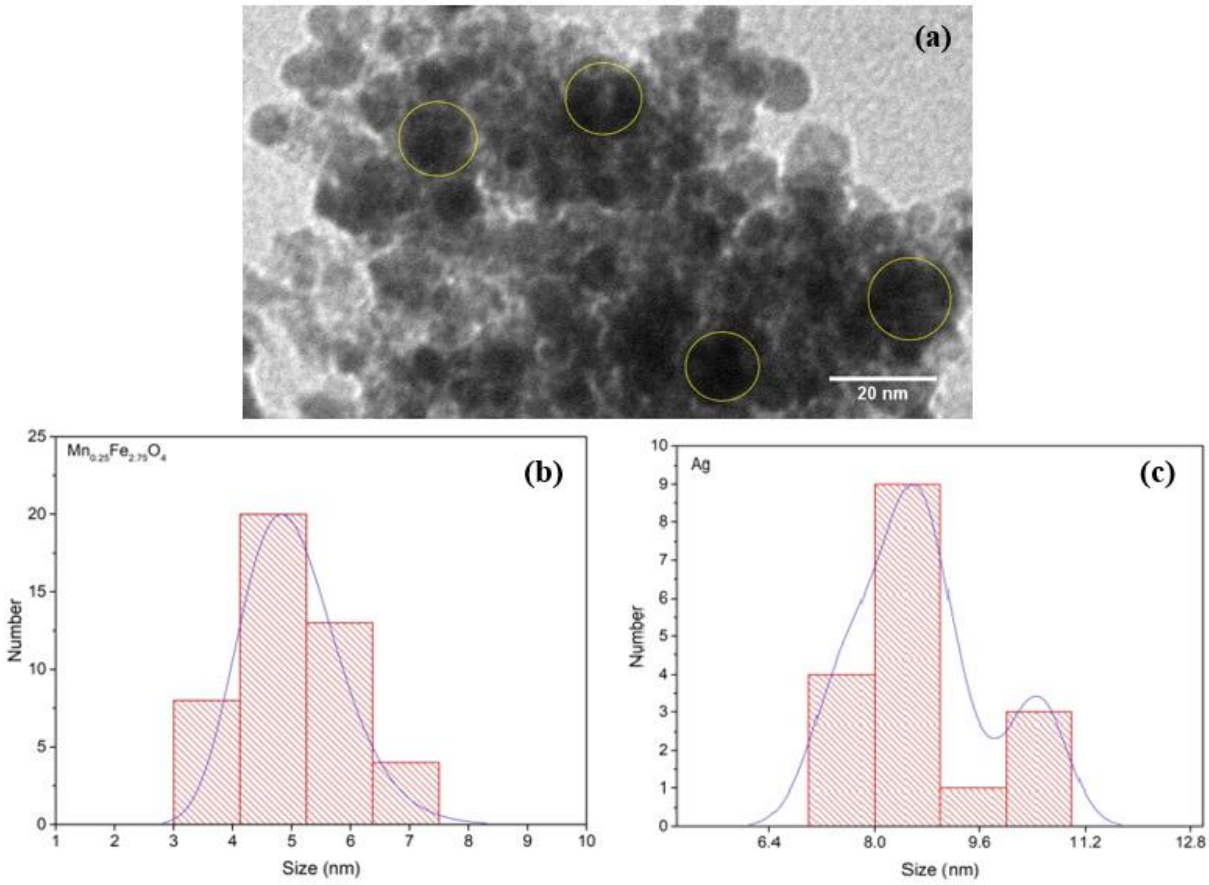

Figure 4. (a) TEM image of $Mn_{0.25}Fe_{2.75}O_4$/Ag nanoparticle composites, (b) histogram of $Mn_{0.25}Fe_{2.75}O_4$ nanoparticle size distribution, and (c) histogram of Ag nanoparticle distribution

3.4. Magneto-thermal Characterization

Magnetic-thermal characterization was successfully carried out by using alternating current frequencies of 553 Hz for 30 minutes by recording data every 3 minutes. The data fitting results against $Mn_{0.25}Fe_{2.75}O_4$ and $Mn_{0.25}Fe_{2.75}O_4$/Ag nanoparticles each is presented in Figure 6 (a) and 6 (b). While the comparison of the experimental data of the two samples is presented in Figure 6 (c).

Based on the data analysis as shown in Figure 6, the Ag nanoparticle composite into $Mn_{0.24}Fe_{2.75}O_4$ nanoparticles can increase the temperature of composite material when the material is under the influence of the AC current magnetic field. On the minute 30, $Mn_{0.25}Fe_{2.75}O_4$ nanoparticle reached the temperature of 9 °C while $Mn_{0.25}Fe_{2.75}O_4$/Ag was able to reach a temperature of 12 °C. This difference has been seen since the third minute where samples with Ag composites showed a significant increase in temperature while samples without Ag composites did not show temperature changes until the sixth minute. After the sixth minute, the two materials both experience an increase in temperature.

From magneto-thermal characterization and data analysis, SAR values of $Mn_{0.25}Fe_{2.75}O_4$ nanoparticles and $Mn_{0.25}Fe_{2.75}O_4$/Ag composites can be determined. The calculation of SAR value was conducted using Equation 1 [32–34].

$$SAR = \left(\frac{\Delta T}{\Delta t}\right)\frac{C}{m} \quad (1)$$

where T is the sample temperature of characterization results, t is the interval time when the measurement was performed, C is the heat capacity constant of sample material, and m is the sample mass. The C heat capacity constant of the sample was obtained from the calculation as in Equation 2 [8].

$$C = \frac{\left(m_{magnetite} \times c_{magnetite}\right) + \left(m_{silver} \times c_{silver}\right)}{m_{total}} \quad (2)$$

with $m_{magnetite}$ and $m_{silver,}$ each was the mass of $Mn_{0.25}Fe_{2.75}O_4$ and the mass of Ag, $c_{magnetite}$ and c_{silver} each was the specific heat capacity of $Mn_{0.25}Fe_{2.75}O_4$ and Ag. The SAR calculation results are presented in Table 1.

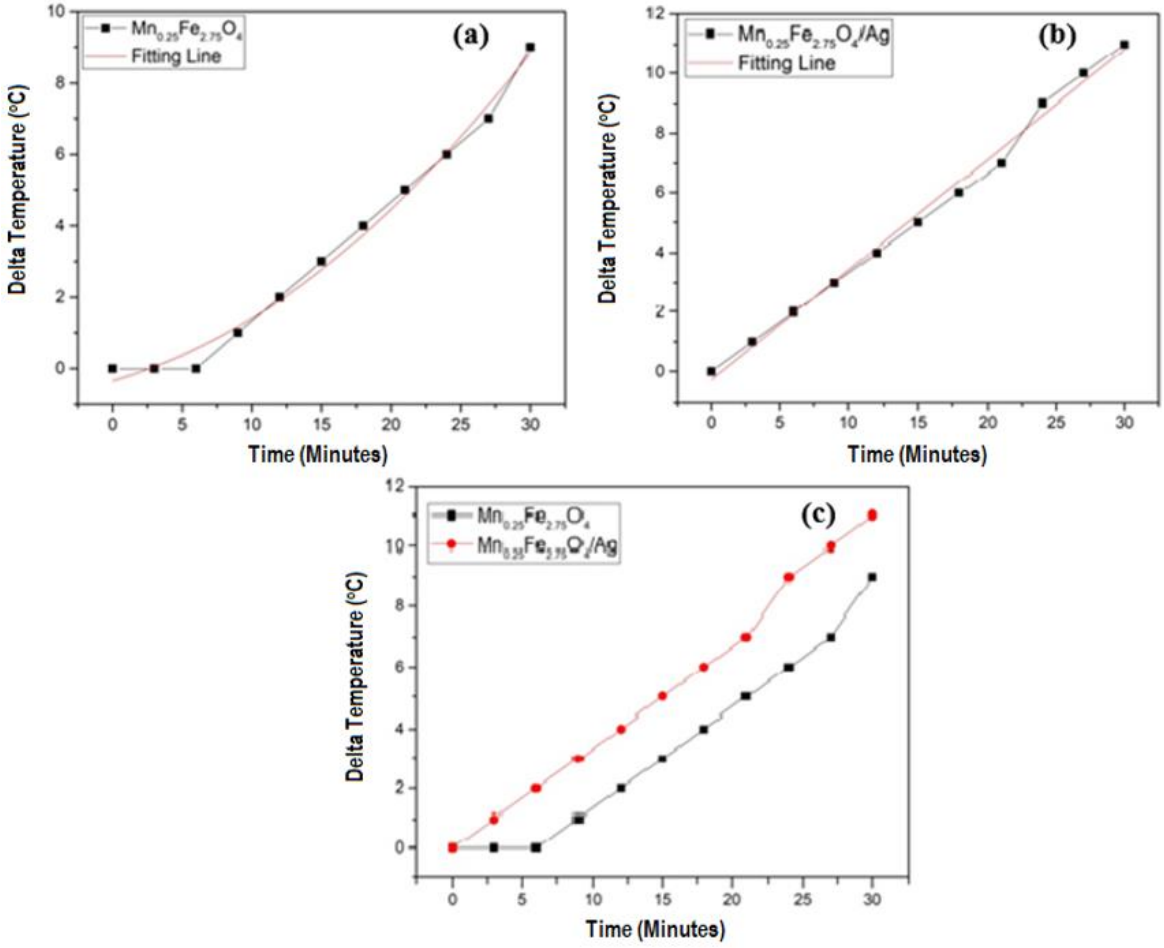

Figure 5. (a) Fitting data of magneto-thermal from $Mn_{0.25}Fe_{2.75}O_4$ Nanoparticles, (b) Fitting data of magneto-thermal from $Mn_{0.25}Fe_{2.75}O_4$/Ag composites, and (c) the data combination of magneto-thermal from $Mn_{0.25}Fe_{2.75}O_4$ and $Mn_{0.25}Fe_{2.75}O_4$/Ag nanoparticles

Table 1. The SAR value of $Mn_{0.25}Fe_{2.75}O_4$ and $Mn_{0.25}Fe_{2.75}O_4$/Ag nanoparticles

Material	Mass of Magnetite (g)	Mass of Silver (g)	Total Mass (g)	*C* (J/gK)	SAR (W/g)
$Mn_{0.25}Fe_{2.75}O_4$	1	0	1	0.651	0.19
$Mn_{0.25}Fe_{2.75}O_4$/Ag	0.8	0.2	1	0.567	0.21

The data in Table 1 showed that the SAR value of $Mn_{0.25}Fe_{2.75}O_4$/Ag composites was greater compared to $Mn_{0.25}Fe_{2.75}O_4$ nanoparticles. These results proved that Ag nanoparticles were relatively effective in increasing the SAR value of $Mn_{0,25}Fe_{2,75}O_4$/Ag composites from 0.19 W/g (without Ag) into 0.21 W/g (with 0.2 g Ag). However, this SAR value is still considered relatively low when

compared to the SAR value obtained by other researchers. Shah et al. [9] report SAR values of magnetic nanoparticles can reach the numbers of 3.7-325 W/g under the influence of a specific magnetic field with the frequency ranged between 123-430 kHz. Then Kekalo, *et al.* [35] explained that the SAR value of gamma-Fe_2O_3 particle was at the range of 22–200 W/g under the influence of alternating magnetic field at the frequency of 160 kHz. Meanwhile, Sathya et al. [36] also showed that the SAR value was not significantly different from the previous research which was 215 W/g with the frequency of alternating magnetic field of 126 kHz for Fe_3O_4 material. The low SAR value obtained from this report was one of them because the frequency used was relatively low compared to previous researchers' reports. Thus, it is necessary to have a high adequate frequency setting to generate SAR values so that they can be effectively applied to biomedical sources.

4. Conclusion

The magnetite material in this study has been synthesized using the coprecipitation method, while the silver material in this study was successfully synthesized by using a chemical reduction method with an NH_4OH reduction. From X-Ray Diffraction data analysis, Mn^{2+} cation has been substituted well in the Fe_3O_4 forming $Mn_{0.25}Fe_{2.75}O_4$ nanoparticles. Besides, Ag nanoparticles have also been successfully composited inside $Mn_{0.25}Fe_{2.75}O_4$ nanoparticles forming $Mn_{0.25}Fe_{2.75}O_4$/Ag material. Based on the magneto-thermal test results, the addition of Ag nanoparticles on $Mn_{0.25}Fe_{2.75}O_4$ nanoparticle can increase the SAR value of SAR $Mn_{0,25}Fe_{2,75}O_4$/Ag composite from 0.19 W/g (without Ag) into 0.21 W/g (with 0.2 g Ag). Therefore, Ag nanoparticle is significantly effective to increase the temperature change in the material and potential to be applied in the biomedical field.

Acknowledgments

The authors would like to convey their deepest gratitude to Universitas Negeri Malang (UM) on their support of the research grant. This research is fully supported by PNBP UM grant on behalf on SN.

References

[1] S. Prabha, M. Lahtinen, and M. Sillanpää, "Colloids and Surfaces A : Physicochemical and Engineering Aspects Green synthesis and characterizations of silver and gold nanoparticles using leaf extract of Rosa rugosa," *Colloids Surf. Physicochem. Eng. Asp.*, vol. 364, no. 1–3, hlm. 34–41, 2010.

[2] C. A. Cezar, "Magnetically Responsive Biomaterials for Enhanced Skeletal Muscle Regeneration," no. May, 2015.

[3] Z. Babak; S. Ronald A. Laser-scribed ferrogel sensor with magnetic particles. U.S. Patent No 9,999,369, 2018.

[4] G. Wang, D. Zhao, N. Li, X. Wang, and Y. Ma, "Drug-loaded poly (ε-caprolactone)/Fe_3O_4 composite microspheres for magnetic resonance imaging and controlled drug delivery," *J. Magn. Magn. Mater.*, vol. 456, hlm. 316–323, Jun 2018.

[5] F. Pourebrahim, M. Ghaedi, K. Dashtian, S. Kheirandish, R. Jannesar, and V. Pezeshkpour, "Preparation of chitosan functionalized end-capped Ag-NPs and composited with Fe_3O_4-NPs: Controlled release to pH-responsive delivery of progesterone and antibacterial activity against *pseudomonas aeruginosa (PAO-1)*," *Appl. Organomet. Chem.*, vol. 32, no. 1, hlm. e3921, Jan 2018.

[6] B. Chudasama, A. K. Vala, N. Andhariya, R. V Upadhyay, and R. V Mehta, "Journal of Magnetism and Magnetic Materials Antifungal activity of multifunctional Fe_3O_4–Ag nanocolloids," *J. Magn. Magn. Mater.*, vol. 323, no. 10, hlm. 1233–1237, 2011.

[7] A. Nayamadi Mahmoodabadi, A. Kompany, and M. Mashreghi, "Characterization, antibacterial and cytotoxicity studies of graphene-Fe_3O_4 nanocomposites and Fe_3O_4 nanoparticles synthesized by a facile solvothermal method," *Mater. Chem. Phys.*, vol. 213, hlm. 285–294, Jul 2018.

[8] L. L. Lao and R. V Ramanujan, "Magnetic and hydrogel composite materials for hyperthermia

applications," vol. 5, hlm. 1061–1064, 2004.
[9] R. R. Shah, T. P. Davis, A. L. Glover, D. E. Nikles, and C. S. Brazel, "Impact of magnetic field parameters and iron oxide nanoparticle properties on heat generation for use in magnetic hyperthermia," *J. Magn. Magn. Mater.*, vol. 387, hlm. 96–106, Agu 2015.
[10] S. M. Ghaseminezhad, S. A. Shojaosadati, and R. L. Meyer, "Ag/Fe_3O_4 nanocomposites penetrate and eradicate S. aureus biofilm in an in vitro chronic wound model," *Colloids Surf. B Biointerfaces*, vol. 163, hlm. 192–200, 2018.
[11] J. Wang, X. Yang, A. Li, and X. Cai, "Preparation and characterization of multifunctional Fe_3O_4-coated Ag nanocomposites for catalytic reduction of 4-nitrophenol," *Mater. Lett.*, vol. 220, hlm. 24–27, 2018.
[12] T. D. Ngo *et al.*, "Antibacterial Nanocomposites Based on Fe_3O_4-Ag Hybrid Nanoparticles and Natural Rubber-Polyethylene Blends," *Int. J. Polym. Sci.*, vol. 2016, 2016.
[13] J. Du and C. Jing, "Preparation of Fe_3O_4@Ag SERS substrate and its application in environmental Cr(VI) analysis," *J. Colloid Interface Sci.*, vol. 358, no. 1, hlm. 54–61, 2011.
[14] S. M. Ghaseminezhad and S. A. Shojaosadati, "Evaluation of the antibacterial activity of Ag/Fe_3O_4 nanocomposites synthesized using starch," *Carbohydr. Polym.*, vol. 144, hlm. 454–463, 2016.
[15] Q. Yin *et al.*, "Plasmonic molybdenum oxide nanosheets supported silver nanocubes for enhanced near-infrared antibacterial activity: Synergism of photothermal effect, silver release and photocatalytic reactions," *Appl. Catal. B Environ.*, vol. 224, hlm. 671–680, Mei 2018.
[16] F. K. Alsammarraie, W. Wang, P. Zhou, A. Mustapha, and M. Lin, "Green synthesis of silver nanoparticles using turmeric extracts and investigation of their antibacterial activities," *Colloids Surf. B Biointerfaces*, vol. 171, hlm. 398–405, Nov 2018.
[17] A. Hoseinzadeh, A. Habibi-yangjeh, and M. Davari, "Progress in Natural Science : Materials International Antifungal activity of magnetically separable Fe_3O_4/ZnO/AgBr nanocomposites prepared by a facile microwave-assisted method," *Prog. Nat. Sci. Mater. Int.*, vol. 26, no. 4, hlm. 334–340, 2016.
[18] A. Taufiq *et al.*, "Nanoscale Clustering and Magnetic Properties of $Mn_xFe_{3-x}O_4$ Particles Prepared from Natural Magnetite," hlm. 2855–2863, 2015.
[19] H. Yoon, J. S. Lee, J. H. Min, J. Wu, and Y. K. Kim, "Synthesis , microstructure , and magnetic properties of monosized $Mn_xZn_yFe_{3-x-y}O_4$ ferrite nanocrystals," no. Iii, hlm. 1–5, 2013.
[20] A. Taufiq, E. G. Rachman Putra, A. Okazawa, I. Watanabe, N. Kojima, and S. Pratapa, "Nanoscale Clustering and Magnetic Properties of $Mn_xFe_{3-x}O_4$ Particles Prepared from Natural Magnetite," *J. Supercond. Nov. Magn.*, vol. 28, no. 9, hlm. 2855–2863, Sep 2015.
[21] J. Amighian, E. Karimzadeh, and M. Mozaffari, "Journal of Magnetism and Magnetic Materials The effect of Mn 2 þ substitution on magnetic properties of $Mn_xFe_{3-x}O_4$ nanoparticles prepared by coprecipitation method," *J. Magn. Magn. Mater.*, vol. 332, hlm. 157–162, 2013.
[22] Y. H. Li *et al.*, "Investigation of cation distribution in single crystalline $Fe_{3-x}Mn_xO_4$ microspheres based on Mössbauer spectroscopy Investigation of cation distribution in single crystalline $Fe_{3-x}Mn_xO_4$ microspheres based on Mo ¨ ssbauer spectroscopy," vol. 544, hlm. 10–13, 2012.
[23] B. D. Cullity and C. D. Graham, "Fine Particles and Thin Films," dalam *Introduction to Magnetic Materials*, John Wiley & Sons, Inc., 2008, hlm. 359–408.
[24] P. Chen *et al.*, "In-situ monitoring reversible redox reaction and circulating detection of nitrite via an ultrasensitive magnetic Au@Ag SERS substrate," *Sens. Actuators B Chem.*, vol. 256, hlm. 107–116, 2018.
[25] L. M. Tung *et al.*, "Synthesis, Characterizations of Superparamagnetic Fe_3O_4–Ag Hybrid Nanoparticles and Their Application for Highly Effective Bacteria Inactivation," *J. Nanosci. Nanotechnol.*, vol. 16, no. 6, hlm. 5902–5912, 2016.
[26] Y. Sun *et al.*, "Controlled synthesis of Fe_3O_4/Ag core-shell composite nanoparticles with high

electrical conductivity," *J. Electron. Mater.*, vol. 41, no. 3, hlm. 519–523, 2012.
[27] E. Tahmasebi and Y. Yamini, "Facile synthesis of new nano sorbent for magnetic solid-phase extraction by self assembling of bis-(2,4,4-trimethyl pentyl)-dithiophosphinic acid on Fe_3O_4@Ag core@shell nanoparticles: Characterization and application," *Anal. Chim. Acta*, vol. 756, hlm. 13–22, 2012.
[28] C. C. *et al.*, "Extracorporeal magnetic approach to reduce the unwanted side-effects and improve antibacterial activity of Ag/Fe_3O_4 nanocomposites in rat," *J. Biomed. Mater. Res. - Part B Appl. Biomater.*, vol. 106, no. 5, hlm. 2029–2036, 2018.
[29] Z. Hassannejad and M. E. Khosroshahi, "Synthesis and evaluation of time dependent optical properties of plasmonic–magnetic nanoparticles," *Opt. Mater.*, vol. 35, no. 3, hlm. 644–651, Jan 2013.
[30] Y. T. Prabhu, K. V. Rao, B. S. Kumari, V. S. S. Kumar, and T. Pavani, "Synthesis of Fe_3O_4 nanoparticles and its antibacterial application," *Int. Nano Lett.*, vol. 5, no. 2, hlm. 85–92, 2015.
[31] S. Venkateswarlu, B. Natesh Kumar, B. Prathima, K. Anitha, and N. V. V Jyothi, "A novel green synthesis of Fe_3O_4-Ag core shell recyclable nanoparticles using Vitis vinifera stem extract and its enhanced antibacterial performance," *Phys. B Condens. Matter*, vol. 457, hlm. 30–35, 2015.
[32] B. Mehdaoui *et al.*., "Optimal Size of Nanoparticles for Magnetic Hyperthermia : A Combined Theoretical and Experimental Study," hlm. 4573–4581, 2011.
[33] K. Murase *et al.*., "Simulation and experimental studies on magnetic hyperthermia with use of superparamagnetic iron oxide nanoparticles," *Radiol. Phys. Technol.*, vol. 4, no. 2, hlm. 194–202, Jul 2011.
[34] S. Huang, S. Wang, A. Gupta, and S. J. Salon, "On the measurement technique for specific absorption rate of nanoparticles in an alternating electromagnetic field," vol. 035701, 2012.
[35] K. Kekalo, I. Baker, R. Meyers, and J. Shyong, "Magnetic Nanoparticles with High Specific Absorption Rate at Low Alternating Magnetic Field," *Nano LIFE*, vol. 5, no. 2, Jun 2015.
[36] A. Sathya, S. Kalyani, S. Ranoo, and J. Philip, "One-step microwave-assisted synthesis of water-dispersible Fe_3O_4 magnetic nanoclusters for hyperthermia applications," *J. Magn. Magn. Mater.*, vol. 439, hlm. 107–113, Okt 2017.